



OPEN ACCESS

EDITED BY

Hao Hu,
China University of Geosciences Wuhan,
China

REVIEWED BY

Xiaodong Deng,
China University of Geosciences Wuhan,
China
Changming Wang,
China University of Geosciences, China
Xiaocui Chen,
Guizhou Institute of Technology, China

*CORRESPONDENCE

Peng Chai,
✉ cx001chaipeng@163.com

RECEIVED 24 December 2022

ACCEPTED 19 April 2023

PUBLISHED 09 May 2023

CITATION

Yuan L, Chai P, Hou Z, Zheng Y and
Quan H (2023), Implications of Nd
isotopic mapping for crustal composition
and metallogenesis in the Sanjiang
orogenic belt (SW China).
Front. Earth Sci. 11:1131338.
doi: 10.3389/feart.2023.1131338

COPYRIGHT

© 2023 Yuan, Chai, Hou, Zheng and
Quan. This is an open-access article
distributed under the terms of the
[Creative Commons Attribution License
\(CC BY\)](https://creativecommons.org/licenses/by/4.0/). The use, distribution or
reproduction in other forums is
permitted, provided the original author(s)
and the copyright owner(s) are credited
and that the original publication in this
journal is cited, in accordance with
accepted academic practice. No use,
distribution or reproduction is permitted
which does not comply with these terms.

Implications of Nd isotopic mapping for crustal composition and metallogenesis in the Sanjiang orogenic belt (SW China)

Lingling Yuan¹, Peng Chai^{1*}, Zengqian Hou¹, Yuanchuan Zheng² and Haihui Quan¹

¹Institute of Geology, Chinese Academy of Geological Sciences (CAGS), Beijing, China, ²State Key Laboratory of Geological Process and Mineral Resources, School of Earth Sciences and Resources, China University of Geosciences Beijing, Beijing, China

The Sanjiang orogenic belt, located in southwestern China and the southeastern Tibetan Plateau, includes a variety of economically important metal deposits. Previous studies have focused on Lu-Hf isotopic mapping to suggest its lithospheric architecture and mineralization. In this study, we provide the results of Nd isotopic mapping and compare them with the results of Hf isotopic mapping based on the similarity of Sm-Nd and Lu-Hf isotope systems, which indicate three juvenile domains with high $\epsilon_{Nd}(t)$ and young Nd model ages within the Eastern Qiangtang-Simao terrane, while presenting negative $\epsilon_{Nd}(t)$ values over the entire horizon. The very negative $\epsilon_{Nd}(t)$ and old Nd model ages found in the Tengchong-Baoshan terrane and Changning-Menglian suture suggest that these terranes are old and might be reworked. The Nd isotopic mapping of the Sanjiang orogenic belt also suggests a relationship between different lithospheric architectures and the locations of distinct ore deposits. Porphyry-skarn Cu-Mo-(Au) deposits occur in the juvenile crust, which has relatively high $\epsilon_{Nd}(t)$ (-3.3-5.1) and young T_{DM} ages, whereas skarn and hydrothermal vein-type W-Sn deposits and Pb-Zn-Cu-Ag deposits are located in the low- $\epsilon_{Nd}(t)$ area.

KEYWORDS

Sanjiang, Nd isotopic mapping, crustal composition, metallogenesis, crustal architecture

1 Introduction

The formation of the continental crust is a major consequence of planetary differentiation and has played a key role in the evolution of life and the climate of this planet (Campbell and Allen, 2008; Couzinié et al., 2016), as well as in the formation of some ore deposits. The deep crust is not only a zone for crust-mantle interactions and material-energy exchange processes but also a source of many felsic magmas and deep geothermal flows (Hou and Zhang, 2015). With the retention, storage, and subduction of mantle-derived magma at the bottom of the crust, the reworking of the old crust, the formation of juvenile material, and the lateral and vertical growth of the lithosphere occur in the deep crust; the mineralized metals are also adjusted for distribution and re-enrichment (Hou et al., 2015; Hou and Zhang, 2015). Thus, for understanding the formation of large mineralized systems and the spatial distribution of the assemblages of mineralized metals, it is critical to reveal the material composition and distribution of the deep lithosphere, in

particular, the distribution of old and juvenile materials (Hou and Zhang, 2015; Hou et al., 2020). In collisional orogenic systems, the formation of the juvenile crust is considered to be relatively unimportant (e.g., Kerrich et al., 2005; Groves and Bierlein, 2007); in fact, large ore deposits are formed (e.g., Hou and Cook, 2009), which are suggested to be associated with the reworking of the old crust, remelting of the juvenile crust, and migration of crustal melts and fluids (e.g., Hou and Cook, 2009; Lu et al., 2013; Hou et al., 2015; Xu et al., 2021).

Whole-rock Sm-Nd and zircon Lu-Hf isotopic mapping has recently been adopted as a tool for evaluating crustal evolution, which estimates the age of continental crust (e.g., DePaolo, 1988; DePaolo et al., 1991; Kovalenko et al., 2004) and constrains the localization of mineral deposits (Mole et al., 2013; Mole et al., 2014; Hou et al., 2015; Champion and Huston, 2016). Typically, the analogous behavior of Lu-Hf and Sm-Nd isotopic systems in mantle-derived magmas is considered to cause the positive correlation between $\epsilon_{\text{Hf}}(t)$ and $\epsilon_{\text{Nd}}(t)$ values (Vervoort and Patchett, 1996). However, Nd-Hf isotopic decoupling has frequently been reported in previous petrological studies (e.g., Bizimis et al., 2004). Thus, comprehensively considering differential isotopic mapping can contribute to the understanding of the formation of the crust. The advantages of zircon Hf isotopic mapping include 1) high metadata precision, as determined *in situ*; and 2) the abundance of data due to its simple analytical process and relatively low cost. Conversely, it should be noted that $\epsilon_{\text{Hf}}(t)$ values from different zircon grains in a sample or different sites in a zircon vary greatly, up to more than ten ϵ units. Thus, the representative values, mostly median data (Wang et al., 2016; Xu et al., 2021) and weighted average data (Hou et al., 2015), for Hf isotopic mapping are distinct according to different authors. However, the whole-rock Nd isotopic value is an objective average of a specific whole-rock sample and can be an unbiased method for the isotopic mapping of large areas and have more advantages than Hf isotope mapping of subjectively selected zircons (Hou and Wang, 2018).

The Sanjiang orogenic belt (SOB) has attracted considerable interest among the scientific community in terms of its orogenesis and metallogenesis (e.g., Yin and Harrison, 2000; Hou et al., 2007; Deng et al., 2014a; Wang et al., 2014). Several studies have focused on Lu-Hf isotopic mapping to suggest the terrane boundary and mineralization of porphyry Cu-Au, orogenic-Au, and rare earth element deposits (Wang et al., 2016; Xu et al., 2021). Du et al. (2016) stressed that the mapping of $\epsilon_{\text{Nd}}(t)$ and $\epsilon_{\text{Hf}}(t)$ using the method of Kriging interpolation proposed that the Changning-Menglian suture was the boundary of two different regional terranes, and indicated the empirical correlation between Nd isotopic mapping and differential mineralization. For instance, the granite-related W-Sn deposits occur in low- $\epsilon_{\text{Nd}}(t)$ and - $\epsilon_{\text{Hf}}(t)$ areas, while the porphyry-skarn Cu-Mo mineralization is found in high positive $\epsilon_{\text{Hf}}(t)$ and higher negative $\epsilon_{\text{Nd}}(t)$ regions.

However, some fundamental issues are not fully explained, for example, the crustal structures and the tectonic evolutionary history reflected by both $\epsilon_{\text{Nd}}(t)$ and T_{DM} values and the relationship between Nd isotopic mapping and further reasons for the appearance of some types of metallic mineralization, such as Pb-Zn-Cu-Ag and W-Sn deposits, as well as the Cu-Mo mineralization mentioned above. These

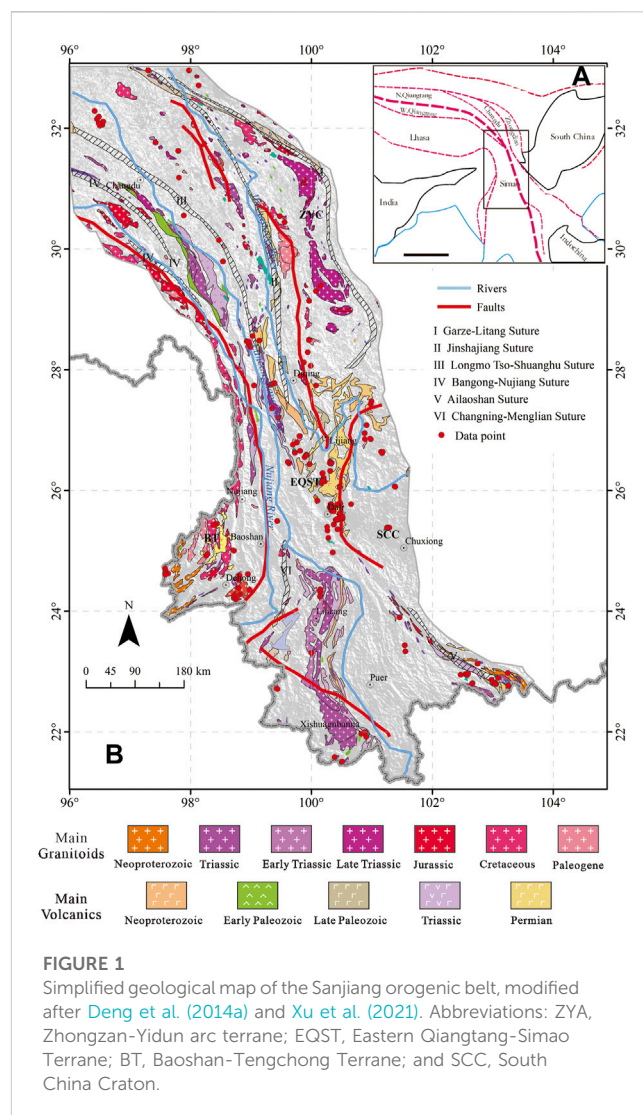


FIGURE 1

Simplified geological map of the Sanjiang orogenic belt, modified after Deng et al. (2014a) and Xu et al. (2021). Abbreviations: ZYA, Zhongzan-Yidun arc terrane; EQST, Eastern Qiangtang-Simao Terrane; BT, Baoshan-Tengchong Terrane; and SCC, South China Craton.

issues are critical for understanding the crustal evolution and spatiotemporal distribution of distinct mineral deposits.

In order to further explain the issues mentioned above, we collected more isotopic data of igneous rocks (665 published whole-rock Rb-Sr and Sm-Nd isotopic analyses), which provided more details about the crustal composition. The isotopic mapping was contoured with the reverse distance weighted interpolation method, which was better for processing the small dataset. Then, we present an overview and re-evaluation of the Cu-Au-(Mo) mineralization, skarn, and hydrothermal vein-type W-Sn and Ag-Cu-Pb-Zn deposits in the SOB. We focus on 1) the spatiotemporal distribution of Nd isotopic data of igneous rocks; 2) the distribution and formation of juvenile and old components; and 3) the relationships between Nd isotopic mapping and different mineralizations.

2 Geological setting

The Sanjiang orogenic belt (SOB) is located within the eastern Himalayan-Tibetan orogen and is composed of three major rivers:

Jinshajiang, Lancangjiang, and Nujiang (Hou et al., 2007; Deng et al., 2014a). Several major continental terranes are preserved in the SOB, including Zhongzan, Eastern Qiangtang, Western Qiangtang, a part of Lhasa, a part of Southern China, Simao, Baoshan, and Tengchong from north to south. The boundaries between the units are major sutures or magma arcs (Deng et al., 2014a; Wang et al., 2014; Deng et al., 2014b). We adopted the “terrane” division scheme of Xu et al. (2021) to simplify the calculation (Figure 1). The Sanjiang orogenic belt is derived from two stages (Deng et al., 2020): accretionary orogenesis in the Palae-Mesozoic with the subduction of the Tethys and collisional orogenesis that began in the Cenozoic (approximately 65 Ma) (Hou et al., 2020).

2.1 Zhongzan-Yidun arc terrane

The Zhongzan-Yidun arc (ZYA) terrane is a combination of the Zhongzan block and the Yidun arc, bound by the Garze-Litang suture to the east and by the Jinshajiang suture to the west (Figure 1). The Zhongzan block could have been derived from the Yangtze block because they have similar Paleozoic stratigraphic sequences and paleontological fossils (Chang, 2000; Xiao et al., 2004), and it is a result of the opening of the Garze-Litang ocean, which is a branch of the Paleo-Tethys (Deng et al., 2020) from the late Paleozoic. The Jinshajiang Ocean is another branch of the Paleo-Tethys and was closed in the Middle Triassic (Deng et al., 2020).

Magmatism in this terrane mainly occurred in the Late Triassic and Late Cretaceous periods (Xiao et al., 2004). The former is found as medium- to high-K calc-alkaline diorite, monzonite, granodiorite, granite, and volcanic rocks (Qu et al., 2002; He et al., 2013; Wu et al., 2014). The latter is mainly found as monzogranite, biotite granite, and granitic porphyry (Qu et al., 2002; Wang et al., 2014).

2.2 Eastern Qiangtang-Simao terrane

The eastern Qiangtang-Simao (EQST) terrane, which extends from north to south, constitutes the main and central parts of the SOB (Figure 1). The Jinshajiang-Ailaoshan suture, which is located to the east of the EQST, was the westward subduction area of the branch of the Paleo-Tethys ocean, while the Longmucuo-Shuanghu-Changning-Menglian suture located to the west was the eastward subduction area of the main Paleo-Tethyan (Deng et al., 2014a; Deng et al., 2014b). The coupling of the subduction of the Proto-Tethys oceanic plate underneath the Simao block and the opening of the Paleo-Tethys ocean suggests that the Eastern Qiangtang and Simao blocks are two Gondwana-derived microcontinents (Usuki et al., 2013; Deng et al., 2014a). The Eastern Qiangtang block was amalgamated with the Western Qiangtang subterrane as the Qiangtang Terrane in the early Jurassic (Hou et al., 2003; Yang et al., 2014) and is the south-central part, while the Lhasa terrane, which is derived from the Australian margin of the Gondwana supercontinent (Zhu et al., 2013), is the southernmost part.

Magmatism in the area developed in the late Permian to very early Triassic in continental-margin arcs, such as the Jomda-Weixi arc along the northern Jinshajiang-Ailaoshan suture (Zi

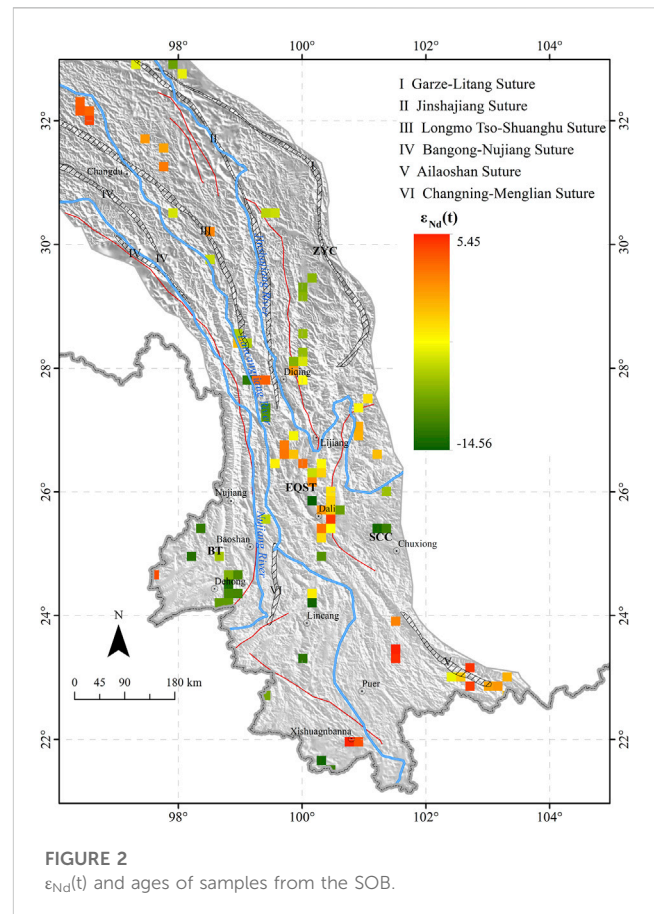


FIGURE 2
 $\epsilon_{Nd}(t)$ and ages of samples from the SOB.

et al., 2012a; Zi et al., 2012b) and the Yaxuanqiao arc in the southern part (Fan et al., 2010; Cai et al., 2014; Xu et al., 2016). The Changning-Menglian Paleo-Tethys subducted beneath the Simao Terrane, resulting in the formation of the Yunxian-Jinggu Arc. This Arc was intruded by the Lincang granitic pluton, which consists of a peraluminous S-type granite with U–Pb zircon aging from 248 to 203 Ma (Peng et al., 2008; Dong et al., 2013; Peng et al., 2013). It is worth noting that the Eocene–Oligocene potassic porphyry intrusions are large and widespread along the Jinshajiang-Red River deep-crustal fault zone in the Eastern Qiangtang block (Yang et al., 2014).

2.3 Baoshan-Tengchong Terrane

The Baoshan-Tengchong (BT) terrane consists of the Baoshan subterrane and Tengchong subterrane, which were once located at the northern margin of Gondwana and accreted to the Eurasian continent in the late Mesozoic (Metcalf, 2006; Jin et al., 2014) (Figure 1). The Baoshan subterrane experienced a similar trend, but the accretionary time might have been in the late Paleozoic to early Mesozoic (Metcalf, 2013). The Changning-Menglian suture located to the east of the BT might have preserved the subduction of the Proto-Tethys and Paleo-Tethys oceanic plates (Deng et al., 2014a; Xu et al., 2021). This suture correlates with the Longmu Tso-Shuanghu Suture in eastern Tibet.

2.4 South China Craton

The South China Craton (SCC) is a block with an Archean history (Gao et al., 1999). Continuous subduction and mantle plume activities following the breakup of the Columbia supercontinent resulted in large volumes of Neoproterozoic volcanic rocks (Xu et al., 2021). The Jinshajiang-Ailaoshan suture, which is accompanied by Eocene–Oligocene alkaline magmatic rocks along the western margin of the SCC (Figure 1), was a result of the India-Asia continental collision during the Cenozoic and lithospheric thickening (Wang et al., 2016; Xu et al., 2021).

3 Petrography of samples

Granitoid and mafic igneous rocks occur widely in the SOB, which consists of several parallel orogens and are the result of distinct orogenic activities (Deng et al., 2013). The collision between India and Asia was initiated at approximately 70–65 Ma (Yin and Harrison, 2000), and the samples collected can be divided into two groups: pre-collisional (≥ 65 Ma) and syn-collisional (< 65 Ma) (Hou et al., 2020). It is important to note that the granite samples or pluton that were heavily contaminated by crustal material may show lower or uneven $\epsilon_{Nd}(t)$ values, thus masking the real information of the crustal component (Maier et al., 2000). These samples with possible bias were excluded from the analyses to present the true distribution of Nd isotopic values. The data points plotted on the map (Figure 2) that have different colors show that the $\epsilon_{Nd}(t)$ values are not very different from other adjacent data points, which could be from the same granite intrusions unless the intrusion ages of the samples are very different. The pre-collisional period covers a long span of time, from the Paleozoic to the entire Mesozoic, and the 79 samples collected were derived from all terranes except the SCC. These samples consisted of monzogranite, granodiorite, granite, leucocratic granite, and gneissose granite.

The other 141 samples collected during the post-collisional period occurred predominantly in the BT and SCC and partly in the EQST; none occurred in the ZYA. The latest U–Pb age of the samples (YS-60) is 22.4 Ma from the Red River shear belt (Zhang and Schaerer, 1999). The lithology of these relatively new samples is similar to that of the older samples and includes leucocratic granite, monzonitic granite porphyry, biotite granite porphyry, granite porphyry, and granite.

Overall, these igneous rocks are widespread in all terranes of the SOB, and their ages were obtained by the U–Pb zircon method. These can be used to constrain the percentage of old continental and young mantle-derived juvenile components at the terrane scale (Wang et al., 2009; Hou et al., 2020).

4 Sr-Nd isotopic characteristics and mapping

4.1 Nd isotopic interpretation

Previously published Nd isotopic data from 220 samples were used to evaluate the crustal evolution in this region over time based on existing zircon U–Pb ages or other isotopic ages, such as Ar–Ar

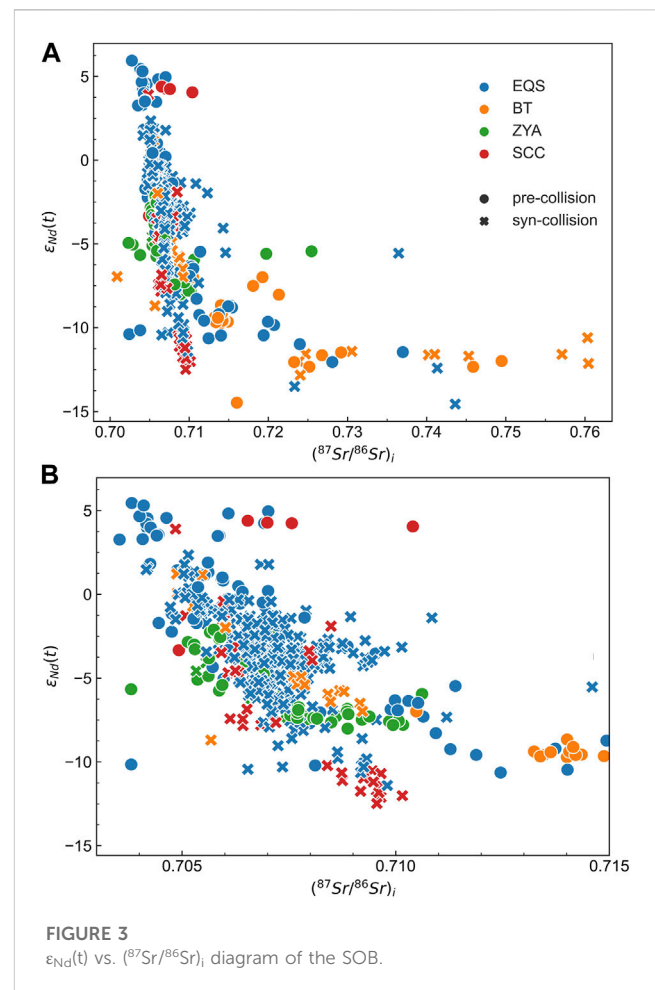


FIGURE 3
 $\epsilon_{Nd}(t)$ vs. $(^{87}Sr/^{86}Sr)_i$ diagram of the SOB.

or K–Ar ages. To produce a data set for the SOB, a consistent method was used to recalculate the data (Maboko and Nakamura, 1996). The specific calculation methods and parameters are as follows (Jacobsen and Wasserburg, 1980; Wu et al., 2002).

$$\epsilon_{Nd}(t) = \left[\frac{(^{143}Nd/^{144}Nd)_i}{(^{143}Nd/^{144}Nd)_{CHUR} - 1} \right] \times 10^4$$

$$(^{143}Nd/^{144}Nd)_i = (^{143}Nd/^{144}Nd) - (^{147}Sm/^{144}Nd)(e^{\lambda t} - 1)$$

$$f_{Sm/Nd} = \frac{(^{147}Sm/^{144}Nd)}{(^{147}Sm/^{144}Nd)_{CHUR} - 1}$$

$$T_{DM1} = \frac{1}{\lambda} \ln \left[1 + \frac{(^{143}Nd/^{144}Nd) - 0.51315}{(^{147}Sm/^{144}Nd) - 0.2137} \right]$$

$$T_{DM2} = T_{DM1} - (T_{DM1} - t)(f_{CC} - f_s) / (f_{CC} - f_{DM})$$

where $\lambda = 6.54 \times 10^{-12}$, $(^{143}Nd/^{144}Nd)_{CHUR} = 0.512638$, $(^{147}Sm/^{144}Nd)_{CHUR} = 0.1967$, $f_{CC} = -0.4$, and $f_{DM} = 0.08592$.

4.2 General characteristics

The data that were collected and recalculated are listed in Supplementary Table S1. The age-corrected initial Sr isotopic ratios showed large variations from 0.700899 to 0.760444 (Figure 3A), but most were between 0.703 and 0.715 (Figure 3B). The $\epsilon_{Nd}(t)$ values varied from -14.56 to 5.94 , and

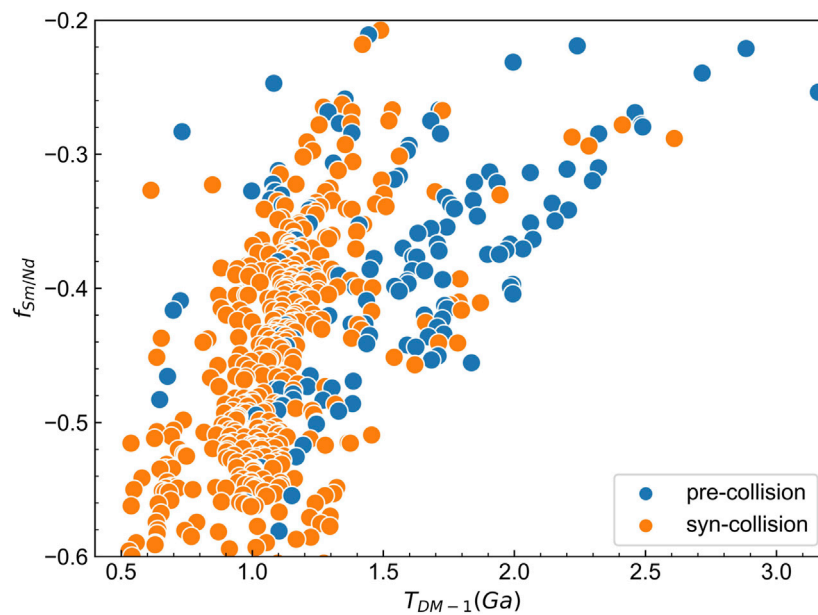


FIGURE 4
 $f_{Sm/Nd}$ vs. T_{DM1} diagram of the SOB.

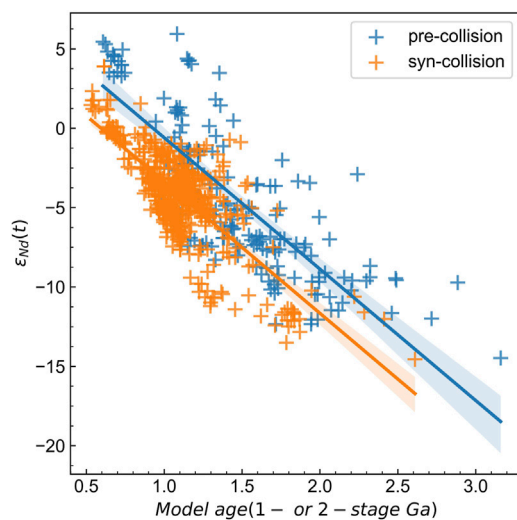


FIGURE 5
 $\epsilon_{Nd}(t)$ vs. the Nd model age; T_{DM2} is used only for samples when $f_{Sm/Nd} > -0.2$ and < -0.6 .

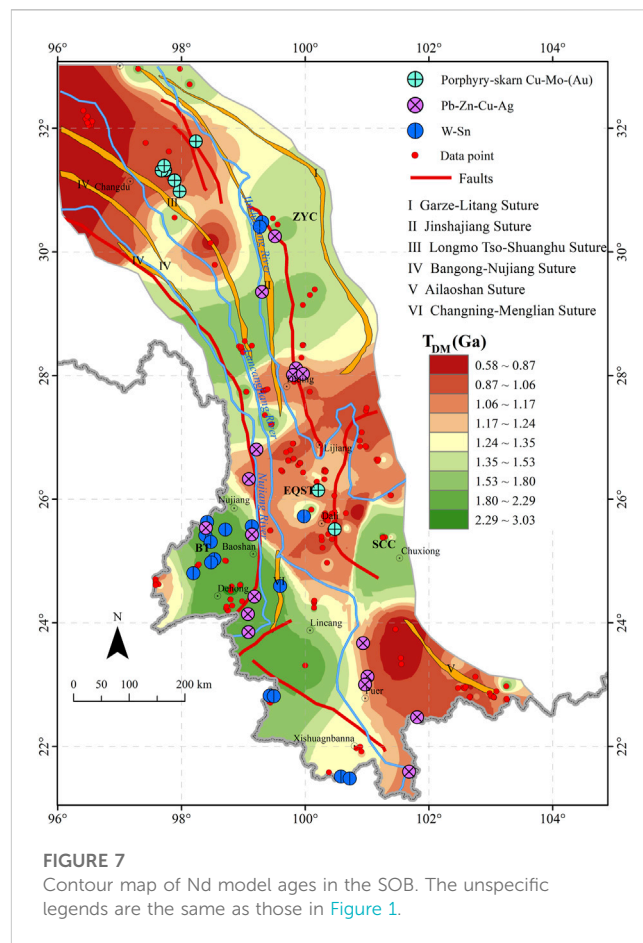
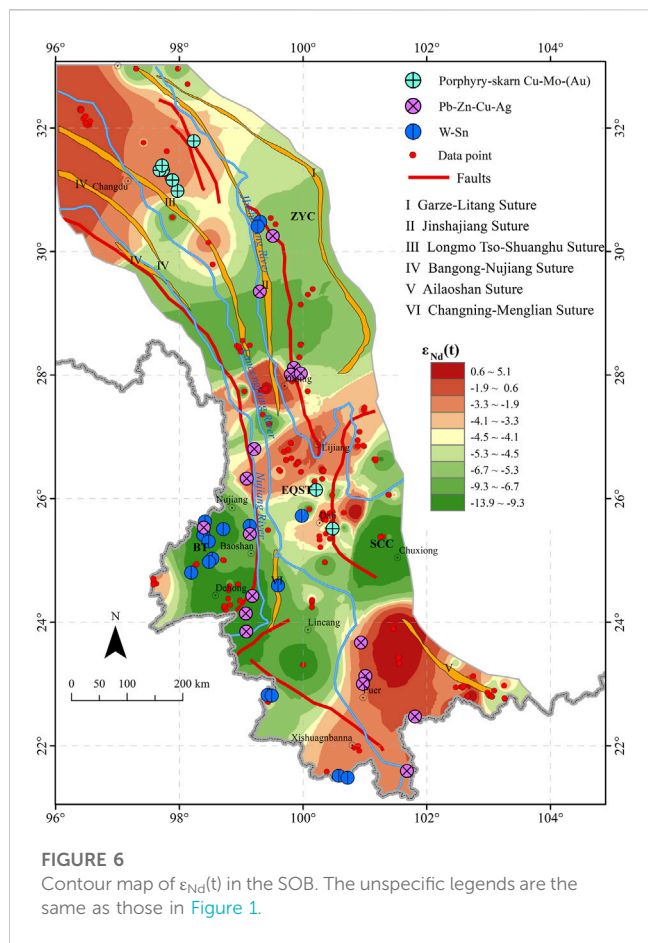
most were <0 and >-10 (Figure 3). Positive $\epsilon_{Nd}(t)$ values from the EQST and SCC terranes were observed to a large extent in mafic rocks, followed by felsic dikes.

Additionally, most samples had one-stage model ages (T_{DM}) between 0.5 and 3.2 Ga, with $f_{Sm/Nd}$ values ranging from -0.68 to 0.75 , and most rocks had $f_{Sm/Nd}$ values between -0.2 and -0.6 (except 55 samples) (Figure 4). The model ages generally become older with increasing $f_{Sm/Nd}$, which shows a linear correlation. Notably, the T_{DM} of the rocks from the syn-collisional stage was

usually younger than that from the pre-collisional stage. As shown in Figure 5, T_{DM2} was applied only to samples with values of $f_{Sm/Nd} > -0.2$ and < -0.6 (Wang et al., 2009). The model age increased with decreasing $\epsilon_{Nd}(t)$ values, which suggests a linear correlation.

4.3 Nd isotopic contour mapping

Since the dataset was small, it was reasonable to apply the inverse distance weighted interpolation method, which uses the 12 nearest neighbors at a “power” (Mole et al., 2014; Hou et al., 2015), in ArcGIS to contour the $\epsilon_{Nd}(t)$ and T_{DM} maps (Wang et al., 2009; Mole et al., 2014; Wang et al., 2016). During the data processing, we attempted to minimize the subjective influence caused by manual screening to show the original distribution of the data as much as possible. All Nd isotope data were classified by the geometric interval method in ArcMap to ensure that the variation between intervals was fairly consistent and that the amount of data in each class range was approximately the same. Particularly, regarding the samples with different Nd isotope values in the same geographical coordinates, the arithmetic mean values were used as the points for mapping to avoid the bias caused by random selection in ArcGIS. As a result, 199 Nd isotopic values were used for mapping. The $\epsilon_{Nd}(t)$ values of rocks in the SOB were mostly negative, while positive values were observed in the southern, northern, and central parts of the EQST. The most negative values of $\epsilon_{Nd}(t)$ occurred in the BT and SCC, and the other areas contained $\epsilon_{Nd}(t)$ values between -9.3 and -1.9 (Figure 6). Similarly, the youngest Nd model ages (0.58–0.87 Ga) occurred in the same position as the $\epsilon_{Nd}(t)$ values in the EQST, and the oldest (2.29–3.03 Ga) was found



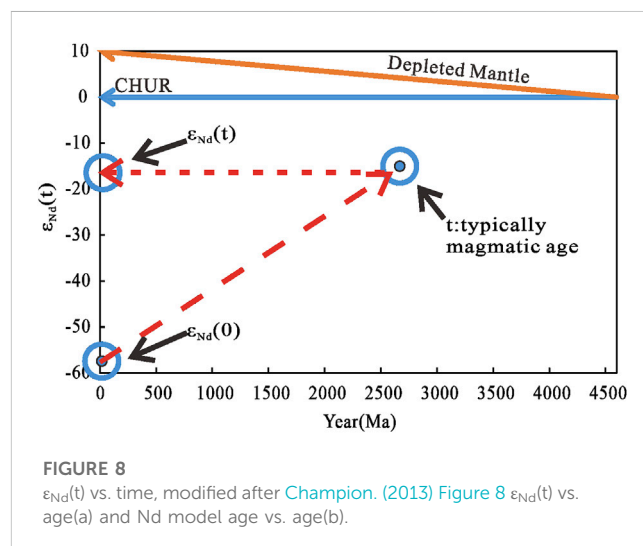
in the SCC and BT, while the other Nd model ages were mostly between 2.29 and 1.17 Ga (Figure 7).

5 Discussion

5.1 Distribution and formation of crustal components

Hf-Nd isotopic data were used to distinguish between juvenile and old crustal components (Wang et al., 2009; Mole et al., 2013; Wang et al., 2016; Granseth et al., 2021; Xu et al., 2021). Juvenile crust, with isotopic values that plot on or close to the depleted mantle evolution line, is regarded as crustal material that is generated directly from the depleted mantle or remelted from material recently extracted from the depleted mantle. In contrast, the old or reworked crust refers to the preexisting crust that was remobilized by partial melting and/or erosion with sedimentation (Belousova et al., 2010; Hawkesworth et al., 2010; Hou et al., 2015). The parent and daughter elements of the Sm-Nd isotope system are both rare earth elements (REEs) and generally behave similarly, which can be used to effectively suggest crustal processes and the source of the rocks in question (DePaolo, 1988; Champion, 2013). During the formation of juvenile crust, the Earth's crust is more enriched in Nd and Sm and has lower Sm/Nd ratios than the complementary depleted mantle reservoir as a result of

lanthanide contraction. In other words, $\epsilon_{Nd}(t)$ values vary over time because of the different Sm/Nd ratios of mantle and crustal reservoirs (Champion, 2013). The values of $\epsilon_{Nd}(t)$ and Nd model ages are tools for distinguishing the possible sources of magma and the formation age of crustal source rocks separately (Hou and Wang, 2018) (Figure 8). A comparison of Hf isotopic mapping from previous studies (Figure 9) and Nd isotopes are discussed below.



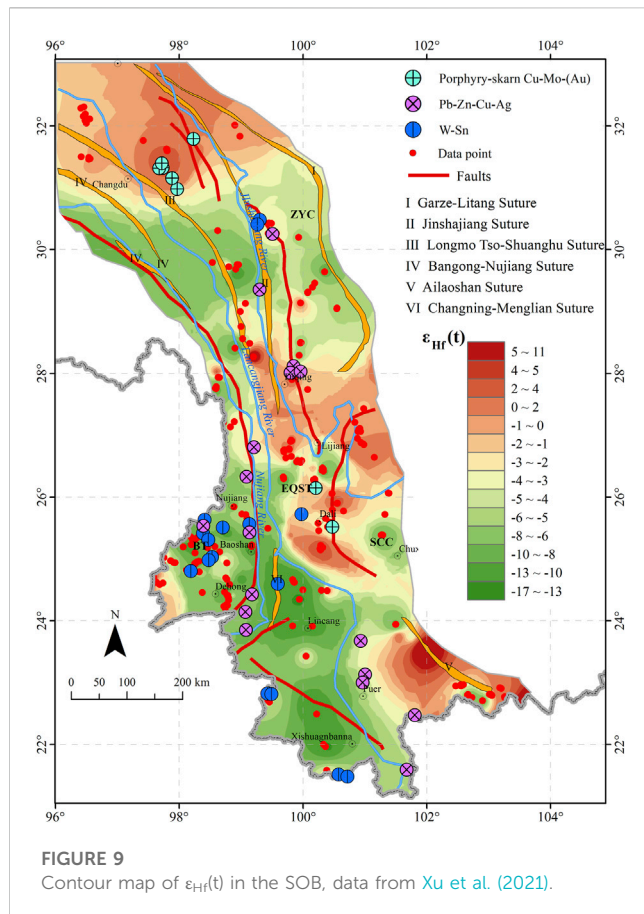


FIGURE 9
Contour map of $\epsilon_{\text{Hf}}(t)$ in the SOB, data from Xu et al. (2021).

5.1.1 The juvenile component

The Nd isotopic system has become an important tool for constraining the age and mechanism of continental formation (Champion and Huston, 2016). For the SOB, high $\epsilon_{\text{Nd}}(t)$ values (> -1.9) occur mostly in three domains, as observed through Hf isotopic mapping (Figure 9), while low $\epsilon_{\text{Nd}}(t)$ values (< -1.9) are observed over the whole horizon (Figure 6).

In the northernmost part of the EQST, high $\epsilon_{\text{Nd}}(t)$ values with low Nd model ages (Figures 6, 7) occur near the Jinshajiang Suture in the east and the Bangong-Nujiang Suture. The ages of samples with high $\epsilon_{\text{Nd}}(t)$ values were between 43 and 37 Ma (Figure 2), while the ages of the other samples around the area varied from 220 to 75 Ma. This indicates either that the juvenile component resulting from the pre-collisional stage shrank or even partially disappeared since the collision transformed the original juvenile crust or that no crust-derived magmatic activity occurred near the Bangonghu-Nujiang suture due to a lack of remelting during the collisional period (Hou et al., 2020). This shows that subduction and collision might have resulted in a continuous accretion of the juvenile component.

In the accretionary orogenic belt, juvenile materials are either collaged in the orogenic belt as a residual oceanic crust or injected into the crust as mantle-derived arc magma, resulting in the formation and growth of continental crust (Hawkesworth et al., 2010). With the subduction of the oceanic lithosphere, the upper continental lithosphere often experiences transformation and destruction; as a result, the old crust might have been subducted

and eroded when the juvenile lower crust was formed (Collins et al., 2011). These geological processes could also have occurred in the Tethys subduction accretionary orogenic stage before the formation of the Tibetan Plateau. During this period, mantle arc magma injection led to vertical crustal growth, and the juvenile crust was preserved in the continental collision orogenic belt as a magma arc and arc root (Zhang et al., 2020).

Similarly, in the center of the EQST, high $\epsilon_{\text{Nd}}(t)$ values occupy a small space where the ages of the samples are approximately 35 Ma (Lu et al., 2013; Liu et al., 2017; Zhou et al., 2019), which is a part of the post-collisional stage. The rock type of these samples includes adakite-like monzogranite, potassic igneous rock, and barren porphyrite, and these felsic rocks were likely formed through crystal fractionation because 1) the felsic rocks have Sr-Nd isotopic components similar to the coeval mafic rocks (shoshonitic rocks) exposed in the western Yangtze (Liu et al., 2017); 2) the mafic rocks have been interpreted to be products of the partial melting of an enriched lithospheric mantle (Guo et al., 2005); and 3) the occurrence of mantle xenoliths (pyroxenite) within the Jianchuan and Xiaoqiaotou intrusions indicates that the source of the rocks should be in the lower thickened crust (approximately 55 km) and that they were derived from an enriched lithospheric mantle source (Zhao et al., 2004). In summary, the coeval shoshonitic and potassic rocks appear to be associated with partial melting of the residual metasomatized lithospheric mantle as well as with the thickened lower crust in the Eocene, which means that continental growth occurred in the post-collisional stage.

In contrast, the $\epsilon_{\text{Nd}}(t)$ values of granites in the BT, which have ages between 53 and 65 Ma, are very positive ($-13.9 \sim -9.3$) (Chen et al., 2007; Chen et al., 2015), while the Nd model ages of the rocks are old (> 1.53 Ga). The source region of these granites, which is different from that cited above, might be the continental crust; in other words, they mainly originated from intracrustal reworking during tectonic events, since almost all isotopic characteristics, such as the old Nd model ages (Figure 8), low $\epsilon_{\text{Hf}}(t)$ values ($-24 \sim -4$) (Chen et al., 2007; Chen et al., 2015) and low $\delta^{18}\text{O}$ values (6.6–8.3‰) (Chen et al., 2015), suggest this possibility.

In the southeasternmost part of the EQST, the highest $\epsilon_{\text{Nd}}(t)$ values correspond to the Ailaoshan Suture and the Yaxuanqiao Arc, and the samples used in this study can be divided into two groups by formation age: ~ 230 Ma (Liu et al., 2014) and ~ 35 Ma (Xin et al., 2020). The former does not contain coeval or earlier mafic-intermediate rocks, which indicates that these granites originated from a basic lower crust (Liu et al., 2014). The latter is similar to the former and lacks the coeval basic components and geochemical characteristics of the thickened lower crust (Xin et al., 2020). The Ailaoshan high-grade metamorphic belt is a complex derived from various petrographic compositions and formation ages. It includes granodiorite dikes (761–829 Ma) (Qi et al., 2012) and mylonitic porphyritic monzogranite (30.95 Ma) (Cao et al., 2012). This belt was intensively deformed by the left-lateral shearing of the Ailaoshan-Red River between 30 and 17 Ma (Tang et al., 2013). However, high $\epsilon_{\text{Nd}}(t)$ values and young Nd model ages do exist in the area, which suggests that some of the materials are from the mantle.

In summary, the juvenile component is relatively dispersed in the SOB and is mainly derived from the post-collisional stage.

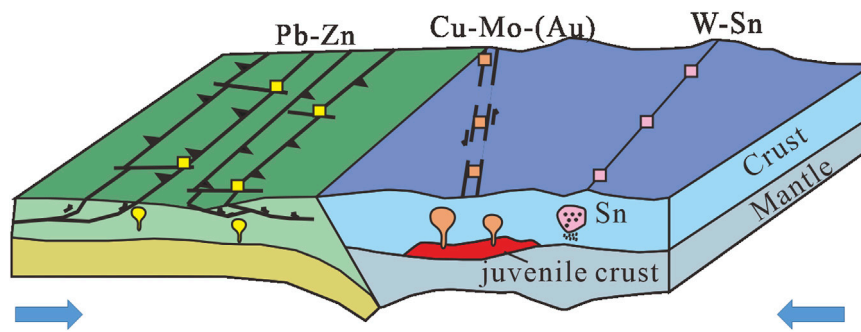


FIGURE 10
Schematic illustration of different deposits, modified after Hou and Zhang (2015).

5.1.2 Old Nd model ages in the SOB

The Nd model ages (T_{DM}) of the sample rocks increase from the east (<1.24 Ga) to the west in the northern part (>1.24 Ga) of the SOB (Figure 6). Although the overall Nd model ages are older than those of the Chinese Altai (Wang et al., 2009), the difference is not great in the north because of the lack of crust-derived magmatic activity in the EQST, which is not discussed below. This pattern also suggests that juvenile material was increasingly added in the eastward direction, which might be evidence of an episodic eastward extrusion of the Tibetan Plateau (Mo et al., 2007). It is worth mentioning that T_{DM} increases with crystallization age in the pre-collisional stage, while it shows fluctuations in the post-collisional stage (Figure 6).

The old Nd model ages boundary corresponds with the results of the contour map of the zircon Hf crustal model ages, which suggests that the Changning-Menglian sutures mark an important boundary that divides the region into an old, reworked crustal block and a juvenile crustal block (Wang et al., 2016). The Changning-Menglian Suture is seen as the boundary between Gondwana to the east and Cathaysia to the west (Kapp et al., 2003; Wang et al., 2016). The distribution of Nd model ages in this study provides additional evidence to support this interpretation.

The ages of the peraluminous samples with old Nd model ages are concentrated in the Ordovician (502–470 Ma) within the BT (Figure 8) (Chen et al., 2007; Liu et al., 2009; Wang et al., 2013), which corresponds with Cambrian-Ordovician magmatic activity along the northern margin of East Gondwana and represents magmatism during the post-Pan-African movement (Yin, 2006; Wang et al., 2012; Zhu et al., 2012; Wang et al., 2015). The source of the rocks with old model ages is the upper crust with contributions from metasedimentary material (Chen et al., 2007; Liu et al., 2009; Wang et al., 2013).

5.2 Nd isotopic mapping and relationships with mineralization

Mo et al. (1993) stressed that the Zhongzan block, sandwiched between the Ganzi-Litang Suture and Jinshajiang Suture, was a breakaway part of the SCC. The old Nd model ages

of granites occurred in the ZYC, which is connected to the upper middle part of the EQST through the Jinshajiang Suture (Figure 7); these granites are mostly near the Yidun Arc, with intrusion ages of 103.7 Ma to 75.2 Ma from the north to the south (Qu et al., 2002), and older granites, such as the Daocheng granite, have an age of 216 Ma (He et al., 2013). The samples from the EQST also have an age of ca. 245 Ma (Wang et al., 2014). The old Nd model age and low $\epsilon_{Nd}(t)$ values may suggest that these felsic rocks originated from the same ancient crust of the SCC basement.

Many metal deposits occur in the SOB to form several metallogenic belts. Figures 6–8 show a strong empirical correlation between the different lithospheric architectures and the locations of distinct ore deposits. All porphyry Cu deposits are confined to juvenile crustal blocks, whereas skarn and hydrothermal vein-type W–Sn deposits are located in the low- $\epsilon_{Nd}(t)$ area, while skarn and hydrothermal vein-type Pb–Zn–Cu–Ag deposits occur between the two types of deposits (Figure 6).

The Cenozoic porphyry-skarn Cu–Mo–(Au) deposits (Wang et al., 2005; Hou et al., 2006; Lu et al., 2013) occur in the juvenile crust within the EQST or along the suture with high $\epsilon_{Nd}(t)$ (–3.3–0) and young T_{DM} ages (0.58–1.17 Ga). Representative porphyry Cu–Mo–(Au) deposits in the SOB are the Machangqing deposit [39 Mt ore, with 0.64% Cu and 56 Mt with 0.08% Mo (Lu et al., 2013)], the Beiya Au deposit [26 Mt ore, with 2.26 g/t Au, (Lu et al., 2013)], and many smaller deposits, such as the Changan, Tongchang, and Yao'an deposits. These deposits are generally associated with potassic-enriched intrusions that were formed in the post-collisional stage (Lu et al., 2013; Lu et al., 2013; Lu et al., 2015). However, no significant porphyry Cu deposits were found in regions with low $\epsilon_{Nd}(t)$ values and old T_{DM} ages. This distribution pattern also occurs in Lhasa Terrane, as revealed by Hf isotopic mapping (Hou et al., 2015). This comparison indicates that the juvenile lower crust might have exerted first-order control on the formation of the porphyry Cu deposits. In the SOB, the juvenile component is mainly derived from the post-collisional stage and characterized by high-K calc-alkaline signatures with high Sr/Y values and $\epsilon_{Nd}(t)$ values (e.g., Lu et al., 2013). Arc magma interacted with the crust in an open environment; then, the fO_2 of magma decreased, which led to the accumulation of

sulfides in the juvenile lower crust. At the post-collision stage, an upwelling of the asthenosphere triggered the melting of metal sulfide-rich crust, which resulted in the release of Cu into the magmatic system as the material source of Cu deposits (Hou et al., 2015). Furthermore, as representatives of the cumulates or residuals of Neoproterozoic arc magmas, the amphibolite xenoliths hosted by the Cenozoic stocks are enriched in Cu and Au (Hou et al., 2017), which reinforces the conclusion that the Cu–Au-enriched low-crustal cumulates might be the metal source of the deposits, so the Cu–Mo–(Au) deposits typically occur at the cratonic edges or sutures.

The W–Sn deposits are mainly located in the BT areas, with negative $\epsilon_{\text{Nd}}(t)$ ($-13\sim-6$) and $\epsilon_{\text{Hf}}(t)$ values, and form the Tengchong-Lianghe Sn metallogenic zone. Previous studies have shown that the occurrence of these deposits tends to occur in the Late Cretaceous to early Eocene (Jiang et al., 2012; Chen et al., 2014; Cao et al., 2017; Sun et al., 2017), which is in concordance with the collisional timeline. A representative deposit, the Lailishan deposit, with an Ar–Ar age of hydrothermal muscovite of 50.4 Ma (Cao et al., 2017), is a large tin deposit located in the midwestern region of Tengchong. The tin orebodies occur in the lower contact zones and the surrounding fractured zones of the granitic intrusion, with a weighted mean U–Pb age of 50.6 Ma (Hou et al., 2007; Cao et al., 2017). The Lailishan granite is characterized by high K, F, and S contents and a high initial $^{87}\text{Sr}/^{87}\text{Sr}$ ratio (Lu and Wang, 1993), and it is rich in Al ($\text{Al}_2\text{O}_3=14.70\%\sim 15.27\%$), alkalis, Ca, REEs, and Ba (Sun et al., 2017), which suggests that the granites are S-type and related to the crustal anatexis. The $\epsilon_{\text{Nd}}(t)$ values are most negative when the T_{DM} ages are the oldest. Both the geochemical characteristics and the results of Nd isotopic mapping suggest that the related igneous rocks are likely derived from the partial melting of predominantly ancient crustal material, which is consistent with the conclusion that S-type magmas are geographically related to W–Sn mineralization (Wang et al., 2014). Correspondingly, the enrichment and mineralization of W–Sn are not only related to the high differentiation of granitic magma but also restricted by the composition of the source area. The origin of W–Sn deposits is the partial melting of the sedimentary rocks, which enriched the metal composition in the muscovite and biotite (Romer and Kroner, 2015). The age of the intrusion is within the syn-collision stage, which means the continental collision and subsequent crustal thickening in the BT resulted in the formation of S-type granites (Zhu et al., 2018) and related W–Sn deposits in the region (Sun et al., 2017).

Skarn and hydrothermal vein-type Pb–Zn–Cu–Ag deposits, such as the enormous Jinding Pb–Zn deposit (200 Mt ore with 6.1% Zn and 1.3% Pb) (Xue et al., 2003; Leach et al., 2017) and the Baiyangping Pb–Zn–Cu–Ag deposit (Xue et al., 2000; Zou et al., 2015), occur within the EQST with relatively low $\epsilon_{\text{Nd}}(t)$ and old T_{DM} ages. The $^{40}\text{Ar}\text{--}^{39}\text{Ar}$ plateau age of silicification quartz in the Baiyangping deposit is 62.7 Ma (Xue et al., 2003), and different age dating methods and samples provide varied ages for the Jinding deposit between 129 and 21 Ma (e.g., Yalikul et al., 2018; Wang et al., 2022). However, almost all the Pb–Zn–Cu–Ag deposits that occur in the area have the Nd isotopic characteristics of old crust, which indicates that the metal source was likely to be crustal materials. Similarly, geochemical and other isotopic characteristics, such as Pb isotope results (Hao et al., 2017), also support this conclusion.

It is worth noting that the formation of the Pb–Zn–Cu–Ag deposits is controlled by trust-nappe structures (Hou et al., 2008).

In summary, the continent-continent collision of India and Asia resulted in the formation of distinct metal deposits based on the different locations and sources of partial melting. The juvenile crust was the base of porphyry-skarn Cu–Mo–(Au) deposits, and the melting of old crust or upper crust contributed to the occurrence of W–Sn deposits and skarn and hydrothermal vein-type Pb–Zn–Cu–Ag deposits controlled by trust-nappe structures (Figure 10).

6 Conclusion

Nd isotopic mapping of the Sanjiang Orogenic Belt reveals that the $\epsilon_{\text{Nd}}(t)$ values in this area are relatively low, but three domains with relatively high $\epsilon_{\text{Nd}}(t)$ values and young Nd model ages occur within the Eastern Qiangtang-Simao Terrane, and the juvenile component in the SOB is mainly derived from the post-collisional stage, which could indicate continental growth. Porphyry-skarn Au–Cu–(Mo) and orogenic deposits are clustered in the relatively juvenile crust. W–Sn and Pb–Zn–Cu–Ag deposits are related to the old crust or upper crust.

Data availability statement

The original contribution presented in the study are included in the article/Supplementary Material, further inquiries can be directed to the corresponding author.

Author contributions

LY and PC, writing and dealing with data; ZH and YZ provided opinions on paper writing; HQ participated in part of map making.

Funding

This work was supported by the National Key Research and Development Program of China (2019YFA0708602, 2022YFF0800903); National Natural Science Foundation of China (41973045, 41602084); Basic Science and Technology Research Fundings of the Institute of Geology, CAGS (J1905); Geological Survey Projects of the China Geological Survey (DD20221647); and the Opening Foundation of the Key Laboratory of Mineral Resources Evaluation in Northeast Asia, Ministry of Land and Resources (DBY-KF-18-02).

Conflict of interest

The authors declare that the research was conducted in the absence of any commercial or financial relationships that could be construed as a potential conflict of interest.

The reviewer CW declared a shared affiliation with the author YZ to the handling editor at time of review.

Publisher's note

All claims expressed in this article are solely those of the authors and do not necessarily represent those of their affiliated organizations, or those of the publisher, the editors and the reviewers. Any product that

may be evaluated in this article, or claim that may be made by its manufacturer, is not guaranteed or endorsed by the publisher.

Supplementary material

The Supplementary Material for this article can be found online at: <https://www.frontiersin.org/articles/10.3389/feart.2023.1131338/full#supplementary-material>

References

- Belousova, E. A., Kostitsyn, Y. A., Griffin, W. L., Begg, G. C., O'Reilly, S. Y., and Pearson, N. J. (2010). The growth of the continental crust: Constraints from zircon Hf-isotope data. *Lithos* 119 (3-4), 457–466. doi:10.1016/j.lithos.2010.07.024
- Bizimis, M., Sen, G., and Salters, V. J. M. (2004). Hf-Nd isotope decoupling in the oceanic lithosphere: Constraints from spinel peridotites from oahu, Hawaii. *Earth Planet. Sci. Lett.* 217 (1-2), 43–58. doi:10.1016/S0012-821X(03)00598-3
- Cai, Y., Wang, Y., Cawood, P. A., Fan, W., Liu, H., Xing, X., et al. (2014). Neoproterozoic subduction along the Ailaoshan zone, South China: Geochronological and geochemical evidence from amphibolite. *Precambrian Res.* 24, 513–528. doi:10.1016/j.precamres.2014.01.009
- Campbell, I. H., and Allen, C. M. (2008). Formation of supercontinents linked to increases in atmospheric oxygen. *Nat. Geosci.* 1, 554–558. doi:10.1038/ngeo259
- Cao, H. W., Pei, Q. M., Zhang, S. T., Zhang, L. K., Tang, L., Lin, J. Z., et al. (2017). Geology, geochemistry and Genesis of the Eocene lailishan Sn deposit in the Sanjiang region, SW China. *J. Asian Earth Sci.* 137, 220–240. doi:10.1016/j.jseas.2017.01.005
- Cao, S., Liu, J., Leiss, B., Vollbrecht, A., Genser, J., Neubauer, F., et al. (2012). Initiation of left-lateral deformation along the ailaoshan - Red River shear zone: New microstructural, textural, and geochronological constraints from the diancang Shan metamorphic massif, SW yunnan, China. *Int. Geol. Rev.* 54, 348–367. doi:10.1080/00206814.2010.543789
- Champion, D. (2013). *Neodymium depleted mantle model age map of Australia: Explanatory notes and user guide*. Australia: Geoscience Australia.
- Champion, D. C., and Huston, D. L. (2016). Radiogenic isotopes, ore deposits and metallogenic terranes: Novel approaches based on regional isotopic maps and the mineral systems concept. *Ore Geol. Rev.* 76, 229–256. doi:10.1016/j.oregeorev.2015.09.025
- Chang, E. Z. (2000). Geology and tectonics of the songpan-ganzi fold belt, southwestern China. *Int. Geol. Rev.* 42 (9), 813–831. doi:10.1080/00206810009465113
- Chen, F., Li, X., Wang, X., Li, Q., and Siebel, W. (2007). Zircon age and Nd-Hf isotopic composition of the Yunnan Tethyan belt, southwestern China. *Int. J. Earth Sci.* 96 (6), 1179–1194. doi:10.1007/s00531-006-0146-y
- Chen, X., Hu, R., Bi, X., Li, H., Lan, J., Zhao, C., et al. (2014). Cassiterite LA-MC-ICP-MS U/Pb and muscovite ⁴⁰Ar/³⁹Ar dating of tin deposits in the Tengchong-Lianghe tin district, NW Yunnan, China. *Miner. Deposita* 49 (7), 843–860. doi:10.1007/s00126-014-0513-8
- Chen, X., Hu, R., Bi, X., Zhong, H., Lan, J., Zhao, C., et al. (2015). Petrogenesis of metaluminous A-type granitoids in the Tengchong-Lianghe tin belt of southwestern China: Evidences from zircon U-Pb ages and Hf-O isotopes, and whole-rock Sr-Nd isotopes. *Lithos* 212–215, 93–110. doi:10.1016/j.lithos.2014.11.010
- Collins, W. J., Belousova, E. A., Kemp, A. I. S., and Murphy, J. B. (2011). Two contrasting Phanerozoic orogenic systems revealed by hafnium isotope data. *Nat. Geosci.* 4 (5), 333–337. doi:10.1038/NNGEO1127
- Couzinié, S., Laurent, O., Moyen, J., Zeh, A., Bouilhol, P., and Villaros, A. (2016). Post-collisional magmatism: Crustal growth not identified by zircon Hf-O isotopes. *Earth Planet. Sci. Lett.* 456, 182–195. doi:10.1016/j.epsl.2016.09.033
- Deng, J., Ge, L., and Yang, L. (2013). Tectonic dynamic system and compound orogeny: Additionally discussing the temporalspatial evolution of Sanjiang orogeny, southwest China. *Acta Petrol. Sin.* 29 (4), 1099–1114.
- Deng, J., Wang, Q., Chen, F., Li, G., Yang, L., Wang, et al. (2020). Further discussion on the Sanjiang Tethyan composite metallogenic system. *Earth Sci. Front.* 27 (2), 106–136.
- Deng, J., Wang, Q., Li, G., Li, C., and Wang, C. (2014a). Tethys tectonic evolution and its bearing on the distribution of important mineral deposits in the Sanjiang region, SW China. *Gondwana Res.* 26 (2), 419–437. doi:10.1016/j.gr.2013.08.002
- Deng, J., Wang, Q., Li, G., and Santosh, M. (2014b). Cenozoic tectono-magmatic and metallogenic processes in the Sanjiang region, southwestern China. *Earth-Science Rev.* 138, 268–299. doi:10.1016/j.earscirev.2014.05.015
- Depaolo, D. J. (1988). Age dependence of the composition of continental crust: Evidence from Nd isotopic variations in granitic rocks. *Earth Planet. Sci. Lett.* 90 (3), 263–271. doi:10.1016/0012-821x(88)90130-6
- Depaolo, D. J., Linn, A. M., and Schubert, G. (1991). The continental crustal age distribution; methods of determining mantle separation ages from Sm-Nd isotopic data and application to the Southwestern United States. *J. Geophys. Res. Solid Earth* 96 (2), 2071–2088. doi:10.1029/90jb02219
- Dong, G., Mo, X., Zhao, Z., Zhu, D., Goodman, R. C., Kong, H., et al. (2013). Zircon U-Pb dating and the petrological and geochemical constraints on Lincang granite in western yunnan, China: Implications for the closure of the Paleo-Tethys ocean. *J. Asian Earth Sci.* 62, 282–294. doi:10.1016/j.jseas.2012.10.003
- Du, B., Wang, C., He, X., Yang, L., Chen, J., Shi, K., et al. (2016). Advances in research of bulk rock Nd and zircon Hf isotopic mappings: Case study of the Sanjiang Tethyan Orogen. *Acta Petrol. Sin.* 32 (8), 2555–2570.
- Fan, W., Wang, Y., Zhang, A., Zhang, F., and Zhang, Y. (2010). Permian arc-back-arc basin development along the Ailaoshan tectonic zone: Geochemical, isotopic and geochronological evidence from the Mojiang volcanic rocks, Southwest China. *Lithos* 119 (3-4), 553–568. doi:10.1016/j.lithos.2010.08.010
- Gao, S., Ling, W., Qiu, Y., Lian, Z., Hartmann, G., and Simon, K. (1999). Contrasting geochemical and Sm-Nd isotopic compositions of archean metasediments from the kongling high-grade terrain of the Yangtze craton: Evidence for cratonic evolution and redistribution of REE during crustal anatexis. *Geochimica Cosmochimica Acta* 63 (13), 2071–2088. doi:10.1016/s0016-7037(99)00153-2
- Granseth, A., Slagstad, T., Roberts, N. M. W., Hagen-Peter, G., Kirkland, C. L., Møkkelgjerd, S. H. H., et al. (2021). Multi-isotope tracing of the 1.3–0.9 Ga evolution of Fennoscandia; crustal growth during the Sveconorwegian orogeny. *Gondwana Res.* 91, 31–39. doi:10.1016/j.gr.2020.10.019
- Groves, D. I., and Bierlein, F. P. (2007). Geodynamic settings of mineral deposit systems. *J. Geol. Soc.* 164 (1), 19–30. doi:10.1144/0016-76492006-065
- Guo, Z., Hertogen, J., Liu, J., Pasteels, P., Boven, A., Punzalan, L., et al. (2005). Potassic magmatism in western sichuan and yunnan provinces, SE Tibet, China: Petrological and geochemical constraints on petrogenesis. *J. Petrology* 46 (1), 33–78. doi:10.1093/petrology/egh061
- Hao, H., Song, Y., Zhuang, T., and Ma, J. (2017). Metal source of Jinding superlarge lead-zinc deposit: Constraint from lead isotopic composition. *Mineral. Deposits* 2, 123–144. doi:10.16111/j.0258-7106.2017.02.008
- Hawkesworth, C. J., Dhuime, B., Pietranik, A. B., Cawood, P. A., Kemp, A. I. S., and Storey, C. D. (2010). The generation and evolution of the continental crust. *J. Geol. Soc.* 167 (2), 229–248. doi:10.1144/0016-76492009-072
- He, D., Zhu, W., Zhong, H., Ren, T., Bai, Z., and Fan, H. (2013). Zircon U-Pb geochronology and elemental and Sr-Nd-Hf isotopic geochemistry of the Daocheng granitic pluton from the Yidun Arc, SW China. *J. Asian Earth Sci.* 67–68, 1–17. doi:10.1016/j.jseas.2013.02.002
- Hou, Z., and Wang, T. (2018). Isotopic mapping and deep material probing(II): Revealing the compositional evolution of the lithosphere and crustal growth processes. *Earth Sci. Front.* 25 (6), 20–41. doi:10.13745/j.esf.2018.11.19
- Hou, Z., and Cook, N. J. (2009). Metallogenesis of the Tibetan collisional orogen: A review and introduction to the special issue. *Ore Geol. Rev.* 36 (1), 2–24. doi:10.1016/j.oregeorev.2009.05.001
- Hou, Z., Duan, L., Lu, Y., Zheng, Y., Zhu, D., Yang, Z., et al. (2015). Lithospheric architecture of the Lhasa terrane and its control on ore deposits in the himalayan-Tibetan orogen. *Econ. Geol. Bull. Soc. Econ. Geol.* 110 (6), 1541–1575. doi:10.2113/econgeo.110.6.1541
- Hou, Z., Ma, H., Khin, Z., Zhang, Y., Wang, M., Wang, Z., et al. (2003). The himalayan yulong porphyry copper belt: Product of large-scale strike-slip faulting in eastern Tibet. *Econ. Geol.* 98 (1), 125–145. doi:10.2113/98.1.125
- Hou, Z., Song, Y., Li, Z., Wang, Z., Yang, Z., Yang, Z., et al. (2008). Thrust-controlled sediments-hosted Pb-Zn-Ag-Cu deposits in eastern and northern margins

- of Tibetan orogenic belt: Geological features and tectonic model. *Mineral. Deposits* 27, 124–144.
- Hou, Z., Zaw, K., Pan, G., Mo, X., Xu, Q., Hu, Y., et al. (2007). Sanjiang Tethyan metallogenesis in S.W. China: Tectonic setting, metallogenic epochs and deposit types. *Ore Geol. Rev.* 31 (1), 48–87. doi:10.1016/j.oregeorev.2004.12.007
- Hou, Z., Zeng, P., Gao, Y., Du, A., and Fu, D. (2006). Himalayan Cu–Mo–Au mineralization in the eastern indo-asian collision zone: Constraints from Re–Os dating of molybdenite. *Miner. Deposita* 41 (1), 33–45. doi:10.1007/s00126-005-0038-2
- Hou, Z., and Zhang, H. (2015). Geodynamics and metallogeny of the eastern Tethyan metallogenetic domain. *Ore Geol. Rev.* 70, 346–384. doi:10.1016/j.oregeorev.2014.10.026
- Hou, Z., Zheng, Y., Lu, Z., Xu, B., Wang, C., and Zhang, H. (2020). Growth, thickening and evolution of the thickened crust of the Tibet Plateau. *Acta Geol. Sin.* 94 (10), 2797–2815.
- Hou, Z., Zhou, Y., Wang, R., Zheng, Y., He, W., Zhao, M., et al. (2017). Recycling of metal-fertilized lower continental crust; origin of non-arc Au-rich porphyry deposits at cratonal edges. *Geol. (Boulder)* 45 (6), 563–566. doi:10.1130/g38619.1
- Jacobsen, B., and Wasserburg, G. J. (1980). Sm–Nd isotopic evolution of chondrites. *Earth Planet. Sci. Lett.* 50 (1), 139–155. doi:10.1016/0012-821X(80)90125-9
- Jiang, B., Gong, Q., Zhang, J., and Ma, N. (2012). Late cretaceous aluminium A-type granites and its geological significance of dasongpo Sn deposit, Tengchong, west yunnan. *Acta Petrol. Sin.* 28 (5), 1477–1492.
- Jin, X., Huang, H., Shi, Y., Zhan, L., Rocha, R., Pais, J., et al. (2014). *Permo-Carboniferous successions of the Tengchong Block, western Yunnan, China; status and problems*. Cham: Springer International Publishing, 767–771. doi:10.1007/978-3-319-04364-7_145
- Kapp, P., Yin, A., Manning, C. E., Harrison, T. M., Taylor, M. H., and Ding, L. (2003). Tectonic evolution of the early Mesozoic blueschist-bearing Qiangtang metamorphic belt, central Tibet. *Tectonics* 22 (4), 1043–1068. doi:10.1029/2002TC001383
- Kerrick, R., Goldfarb, R. J., and Richards, J. P. R. (2005). “Metallogenic provinces in an evolving geodynamic framework,” in *One hundredth anniversary volume* (Society of Economic Geologists). doi:10.5382/AV100.33
- Kovalenko, V. I., Yarmolyuk, V. V., Kovach, V. P., Kotov, A. B., Kozakov, I. K., Salnikova, E. B., et al. (2004). Isotope provinces, mechanisms of generation and sources of the continental crust in the central asian mobile belt: Geological and isotopic evidence. *J. Asian Earth Sci.* 23 (5), 605–627. doi:10.1016/S1367-9120(03)00130-5
- Leach, D. L., Song, Y., and Hou, Z. (2017). The world-class jinding Zn–Pb deposit: Ore formation in an evaporite dome, lanping basin, yunnan, China. *Miner. Deposita* 52 (3), 281–296. doi:10.1007/s00126-016-0668-6
- Liu, H., Wang, Y., Fan, W., Zi, J., Cai, Y., and Yang, G. (2014). Petrogenesis and tectonic implications of Late-Triassic high $\epsilon_{Nd(t)}-\epsilon_{Hf(t)}$ granites in the Ailaoshan tectonic zone (SW China). *Sci. China Earth Sci.* 57 (9), 2181–2194. doi:10.1007/s11430-014-4854-z
- Liu, S., Hu, R., Gao, S., Feng, C., Huang, Z., Lai, S., et al. (2009). U–Pb zircon, geochemical and Sr–Nd–Hf isotopic constraints on the age and origin of early palaeozoic I-type granite from the tengchong–baoshan block, western yunnan province, SW China. *J. Asian Earth Sci.* 36 (2–3), 168–182. doi:10.1016/j.jseas.2009.05.004
- Liu, Z., Liao, S., Wang, J., Ma, Z., Liu, Y., Wang, D., et al. (2017). Petrogenesis of late Eocene high Ba–Sr potassic rocks from Western Yangtze block, se Tibet: A magmatic response to the indo-asian collision. *J. Asian Earth Sci.* 135, 95–109. doi:10.1016/j.jseas.2016.12.030
- Lu, B., and Wang, Z. (1993). *Granitoid and related mineralization in the Sanjiang region*. Beijing: Geological Publishing House, 258pp.
- Lu, Y., Campbell Mccuaig, T., Li, Z., Jourdan, F., Hart, C. J. R., Hou, Z., et al. (2015). Paleogene post-collisional lamprophyres in Western Yunnan, Western Yangtze Craton: Mantle source and tectonic implications. *Lithos* 233, 139–161. doi:10.1016/j.lithos.2015.02.003
- Lu, Y. J., Kerrich, R., Mccuaig, T. C., Li, Z. X., Hart, C. J. R., Cawood, P. A., et al. (2013b). Geochemical, Sr–Nd–Pb, and zircon Hf–O isotopic compositions of eocene-oligocene shoshonitic and potassic adakite-like felsic intrusions in western yunnan, SW China: Petrogenesis and tectonic implications. *J. Petrology* 54 (7), 1309–1348. doi:10.1093/petrology/egt013
- Lu, Y., Kerrich, R., Kemp, A. I. S., Mccuaig, T. C., Hou, Z., Hart, C. J. R., et al. (2013a). Intracontinental Eocene–Oligocene porphyry Cu mineral systems of Yunnan, Western Yangtze Craton, China; compositional characteristics, sources, and implications for continental collision metallogeny. *Econ. Geol. Bull. Soc. Econ. Geol.* 108 (7), 1541–1576. doi:10.2113/econgeo.108.7.1541
- Maboko, M. A. H., and Nakamura, E. (1996). Nd and Sr isotopic mapping of the Archaean–Proterozoic boundary in southeastern Tanzania using granites as probes for crustal growth. *Precambrian Res.* 77 (1), 105–115. doi:10.1016/0301-9268(95)00048-8
- Maier, W. D., Arndt, N. T., and Curl, E. A. (2000). Progressive crustal contamination of the Bushveld Complex; evidence from Nd isotopic analyses of the cumulate rocks. *Contributions mineralogy petrology* 140 (3), 316–327. doi:10.1007/s004100000186
- Metcalf, I. (2013). Gondwana dispersion and Asian accretion; tectonic and palaeogeographic evolution of eastern Tethys. *J. Asian earth Sci.* 66, 1–33. doi:10.1016/j.jseas.2012.12.020
- Metcalf, I. (2006). Palaeozoic and mesozoic tectonic evolution and palaeogeography of East asian crustal fragments: The Korean peninsula in context. *Gondwana Res.* 9 (1–2), 24–46. doi:10.1016/j.gr.2005.04.002
- Mo, X., Zhao, Z., Deng, J., Yu, X., Luo, Z., and Dong, G. (2007). Migration of the Tibetan cenozoic potassic volcanism and its transition to eastern basaltic province: Implications for the crustal and mantle flow. *Geoscience* 21 (2), 255–264.
- Mole, D. R., Fiorentini, M. L., Cassidy, K. F., Kirkland, C. L., Thebaud, N., Mccuaig, T. C., et al. (2013). Crustal evolution, intra-cratonic architecture and the metallogeny of an Archaean craton. *Geol. Soc. Spec. Publ.* 393 (1), 23–80. doi:10.1144/SP393.8
- Mole, D. R., Fiorentini, M. L., Thebaud, N., Cassidy, K. F., Mccuaig, T. C., Kirkland, C. L., et al. (2014). Archaean komatiite volcanism controlled by the evolution of early continents. *Proc. Natl. Acad. Sci.* 111 (28), 10083–10088. doi:10.1073/pnas.1400273111
- Peng, T., Wang, Y., Zhao, G., Fan, W., and Peng, B. (2008). Arc-like volcanic rocks from the southern Lancangjiang zone, SW China: Geochronological and geochemical constraints on their petrogenesis and tectonic implications. *Lithos* 102 (1–2), 358–373. doi:10.1016/j.lithos.2007.08.012
- Peng, T., Wilde, S. A., Wang, Y., Fan, W., and Peng, B. (2013). Mid-triassic felsic igneous rocks from the southern Lancangjiang zone, sw China: Petrogenesis and implications for the evolution of paleo-tethys. *Lithos* 168–169, 15–32. doi:10.1016/j.lithos.2013.01.015
- Qi, X., Zeng, L., Zhu, L., Hu, Z., and Hou, K. (2012). Zircon U–Pb and Lu–Hf isotopic systematics of the daping plutonic rocks: Implications for the neoproterozoic tectonic evolution of the northeastern margin of the indochina block, southwest China. *Gondwana Res.* 21 (1), 180–193. doi:10.1016/j.gr.2011.06.004
- Qu, X., Hou, Z., and Zhou, S. (2002). Geochemical and Nd, Sr isotopic study of the post-orogenic granites in the Yidun Arc belt of northern Sanjiang region, southwestern China. *Resour. Geol.* 52 (2), 163–172. doi:10.1111/j.1751-3928.2002.tb00128.x
- Romer, R. L., and Kroner, U. (2015). Sediment and weathering control on the distribution of Paleozoic magmatic tin–tungsten mineralization. *Miner. Deposita* 50 (3), 327–338. doi:10.1007/s00126-014-0540-5
- Sun, Z., Dong, G., Zhao, Z., Wang, W., and Liu, S. (2017). Petrological, geochemical and geochronological features of Lailishan gneissoids in Western Yunnan and their Genesis of partial melting of crustal source. *Geol. China* 44 (6), 1140–1158.
- Tang, Y., Liu, J., Tran, M., Song, Z., Wu, W., Zhang, Z., et al. (2013). Timing of left-lateral shearing along the ailao Shan–Red River shear zone: Constraints from zircon U–Pb ages from granitic rocks in the shear zone along the ailao Shan range, western yunnan, China. *Int. J. Earth Sci.* 102 (3), 605–626. doi:10.1007/s00531-012-0831-y
- Usuki, T., Lan, C., Wang, K., and Chiu, H. (2013). Linking the indochina block and Gondwana during the early paleozoic: Evidence from U–Pb ages and Hf isotopes of detrital zircons. *Tectonophysics* 586, 145–159. doi:10.1016/j.tecto.2012.11.010
- Vervoort, J. D., and Patchett, P. J. (1996). Behavior of hafnium and neodymium isotopes in the crust; constraints from Precambrian crustally derived granites. *Geochimica cosmochimica acta* 60 (19), 3717–3733. doi:10.1016/0016-7037(96)00201-3
- Wang, C., Bagas, L., Lu, Y., Santosh, M., Du, B., and Mccuaig, T. C. (2016). Terrane boundary and spatio-temporal distribution of ore deposits in the Sanjiang tethyan orogen: Insights from zircon Hf-isotopic mapping. *Earth-Science Rev.* 156, 39–65. doi:10.1016/j.earscirev.2016.02.008
- Wang, C., Deng, J., Carranza, E. J. M., and Santosh, M. (2014a). Tin metallogenesis associated with granitoids in the southwestern Sanjiang Tethyan Domain: Nature, deposit types, and tectonic setting. *Gondwana Res.* 26 (2), 576–593. doi:10.1016/j.gr.2013.05.005
- Wang, C., Duan, H., Li, C., Zhu, J., Shi, K., Chen, Q., et al. (2022). Research advance in geochronology of the Mississippi Valley-type Pb–Zn deposits: Debate on the metallogenic age of the jinding deposit. *Acta Petrol. Sin.* 38 (6), 1577–1594. doi:10.18654/1000-0569/2022.06.02
- Wang, D., Qu, W., Li, Z., Yin, H., and Chen, Y. (2005). Mineralization episode of porphyry copper deposits in the Jinshajiang–Red River mineralization belt: Re–Os dating. *Sci. China Ser. D Earth Sci.* 48 (2), 192–198. doi:10.1360/03yd0200
- Wang, T., Jahn, B., Kovach, V. P., Tong, Y., Hong, D., and Han, B. (2009). Nd–Sr isotopic mapping of the Chinese Altai and implications for continental growth in the Central Asian Orogenic Belt. *Lithos* 110 (1), 359–372. doi:10.1016/j.lithos.2009.02.001
- Wang, X., Bi, X., Leng, C., Zhong, H., Tang, H., Chen, Y., et al. (2014b). Geochronology and geochemistry of Late Cretaceous igneous intrusions and Mo–Cu–(W) mineralization in the southern Yidun Arc, SW China: Implications for metallogenesis and geodynamic setting. *Ore Geol. Rev.* 61, 73–95. doi:10.1016/j.oregeorev.2014.01.006
- Wang, X., Zhang, J., Santosh, M., Liu, J., Yan, S., and Guo, L. (2012). Andean-type orogeny in the himalayas of south Tibet: Implications for early paleozoic tectonics along the Indian margin of Gondwana. *Lithos* 154, 248–262. doi:10.1016/j.lithos.2012.07.011
- Wang, Y., Li, S., Ma, L., Fan, W., Cai, Y., Zhang, Y., et al. (2015). Geochronological and geochemical constraints on the petrogenesis of early Eocene metagabbroic rocks in nabang (SW yunnan) and its implications on the neotethyan slab subduction. *Gondwana Res.* 27 (4), 1474–1486. doi:10.1016/j.gr.2014.01.007
- Wang, Y., Xing, X., Cawood, P. A., Lai, S., Xia, X., Fan, W., et al. (2013). Petrogenesis of early paleozoic peraluminous granite in the sibusu block of SW yunnan and diachronous accretionary orogenesis along the northern margin of Gondwana. *Lithos* 182–183, 67–85. doi:10.1016/j.lithos.2013.09.010

- Wu, F., Sun, D., Li, H., Bor-Ming, J., and S, W. (2002). A-type granites in northeastern China; age and geochemical constraints on their petrogenesis. *Chem. Geol.* 187 (1-2), 143–173. doi:10.1016/s0009-2541(02)00018-9
- Wu, T., Xiao, L., Gao, R., Yang, H., and Yang, G. (2014). Petrogenesis and tectonic setting of the Queershan composite granitic pluton, eastern Tibetan Plateau: Constraints from geochronology, geochemistry and Hf isotope data. *Sci. China Earth Sci.* 57, 2712–2725. doi:10.1007/s11430-014-4936-y
- Xiao, L., Xu, Y., Xu, J., He, B., and Franco, P. (2004). Chemostratigraphy of flood basalts in the garzê-litang region and zongza block: Implications for western extension of the emeishan large igneous province, SW China. *Acta Geol. Sin. - Engl. Ed.* 78 (1), 61–67.
- Xin, W., Sun, F., Xu, Z., Lu, Y., Zhang, Y., Deng, J., et al. (2020). Potassic/ultrapotassic intrusions at the southwestern margin of the Yangtze Craton, southwestern China: Petrogenesis and implications for the metal and fluid source of non-arc porphyry Cu–(Mo–Au) deposits, *Lithos* 352–353, 105294–105353. doi:10.1016/j.lithos.2019.105294
- Xu, B., Hou, Z., Griffin, W. L., Zheng, Y., Wang, T., Guo, Z., et al. (2021). Cenozoic lithospheric architecture and metallogenesis in Southeastern Tibet. *Earth-Science Rev.* 214, 103472. doi:10.1016/j.earscirev.2020.103472
- Xu, L., Bi, X., Hu, R., Qi, Y., Tang, Y., Wang, X., et al. (2016). Redox states and Genesis of magmas associated with intra-continental porphyry Cu–Au mineralization within the Jinshajiang–Red River alkaline igneous belt, SW China. *Ore Geol. Rev.* 73, 330–345. doi:10.1016/j.oregeorev.2015.05.007
- Xue, C., Chen, Y., Wang, D., Yang, J., Yang, W., and Zeng, R. (2003). Geology and isotopic composition of helium, neon, xenon and metallogenic age of the Jinding and Baiyangping ore deposits, northwest Yunnan, China. *Sci. China (Series D)* 8 (46), 789–800. doi:10.1007/bf02879523
- Xue, C., Wang, D., Chen, Y., Yang, J., and Yang, W. (2000). Helium, argon, and xenon isotopic compositions of ore-forming fluids in jinding-baiyangping polymetallic deposits, yunnan, southwest China. *Acta Geol. Sin. - Engl. Ed.* 74 (3), 521–528.
- Yalikun, Y., Xue, C., and Symons, D. T. A. (2018). Paleomagnetic age and tectonic constraints on the Genesis of the giant Jinding Zn–Pb deposit, Yunnan, China. *Miner. Deposita* 53 (2), 245–259. doi:10.1007/s00126-017-0733-9
- Yang, Z., Hou, Z., Xu, J., Bian, X., Wang, G., Yang, Z., et al. (2014). Geology and origin of the post-collisional Narigongma porphyry Cu–Mo deposit, southern Qinghai, Tibet. *Gondwana Res.* 26 (2), 536–556. doi:10.1016/j.gr.2013.07.012
- Yin, A. (2006). Cenozoic tectonic evolution of the Himalayan orogen as constrained by along-strike variation of structural geometry, exhumation history, and foreland sedimentation. *Earth-Science Rev.* 76, 1–131. doi:10.1016/j.earscirev.2005.05.004
- Yin, A., and Harrison, T. M. (2000). Geologic evolution of the himalayan-Tibetan orogen. *Annu. Rev. Earth Planet. Sci.* 28, 211–280. doi:10.1146/annurev.earth.28.1.211
- Zhang, L., and Schaerer, U. (1999). Age and origin of magmatism along the Cenozoic Red River shear belt, China. *Contributions mineralogy petrology* 134 (1), 67–85. doi:10.1007/s004100050469
- Zhang, Z., Ding, H., Palin, R. M., Dong, X., Tian, Z., and Chen, Y. (2020). The lower crust of the Gangdese magmatic arc, southern Tibet, implication for the growth of continental crust. *Gondwana Res.* 77, 136–146. doi:10.1016/j.gr.2019.07.010
- Zhao, X., Yu, X., Mo, X., Zhang, J., and Lv, B. (2004). Petrological and geochemical characteristics of cenozoic alkali-rich porphyries and xenoliths hosted in western yunnan province. *Geoscience* 2, 217–228. doi:10.3969/j.issn.1000-8527.2004.02.012
- Zhou, Y., Xu, B., Hou, Z. Q., Wang, R., Zheng, Y. C., and He, W. Y. (2019). Petrogenesis of Cenozoic high–Sr/Y shoshonites and associated mafic microgranular enclaves in an intracontinental setting: Implications for porphyry Cu–Au mineralization in Western Yunnan, China. *Lithos* 324–325, 39–54. doi:10.1016/j.lithos.2018.10.031
- Zhu, D., Zhao, Z., Niu, Y., Dilek, Y., Hou, Z., and Mo, X. (2013). The origin and pre-Cenozoic evolution of the Tibetan Plateau. *Gondwana Res.* 23 (4), 1429–1454. doi:10.1016/j.gr.2012.02.002
- Zhu, D., Zhao, Z., Niu, Y., Dilek, Y., Wang, Q., Ji, W., et al. (2012). Cambrian bimodal volcanism in the Lhasa Terrane, southern Tibet: Record of an early Paleozoic Andean-type magmatic arc in the Australian proto-Tethyan margin. *Chem. Geol.* 328, 290–308. doi:10.1016/j.chemgeo.2011.12.024
- Zhu, R., Lai, S., Qin, J., Zhao, S., and Santosh, M. (2018). Strongly peraluminous fractionated S-type granites in the Baoshan Block, SW China: Implications for two-stage melting of fertile continental materials following the closure of Bangong-Nujiang Tethys. *Lithos* 316–317, 178–198. doi:10.1016/j.lithos.2018.07.016
- Zi, J., Cawood, P. A., Fan, W., Tohver, E., Wang, Y., and Mccuaig, T. C. (2012a). Generation of Early Indosinian enriched mantle-derived granitoid pluton in the Sanjiang Orogen (SW China) in response to closure of the Paleo-Tethys. *Lithos* 140–141, 166–182. doi:10.1016/j.lithos.2012.02.006
- Zi, J., Cawood, P. A., Fan, W., Wang, Y., Tohver, E., Mccuaig, T. C., et al. (2012b). Triassic collision in the Paleo-Tethys Ocean constrained by volcanic activity in SW China. *Lithos* 144–145, 145–160. doi:10.1016/j.lithos.2012.04.020
- Zou, Z., Hu, R., Bi, X., Wu, L., Feng, C., and Tang, Y. (2015). Absolute and relative dating of Cu and Pb–Zn mineralization in the baiyangping area, yunnan province, SW China: Sm–Nd geochronology of calcite. *Geochem. J.* 49 (1), 103–112. doi:10.2343/geochemj.2.0334